A Luminescent Mixed-Lanthanide-Organic Framework Sensor for Decoding Different Volatile Organic Molecules

ARTICLE *in* ANALYTICAL CHEMISTRY · JUNE 2014

Impact Factor: 5.64 · DOI: 10.1021/ac5013442 · Source: PubMed

5 AUTHORS, INCLUDING:

Chao Zou

South University of Science and Technology of…

19 PUBLICATIONS **1,282** CITATIONS

SEE PROFILE

analytical chemistry

Article

pubs.acs.org/ac

A Luminescent Mixed-Lanthanide-Organic Framework Sensor for Decoding Different Volatile Organic Molecules

Chao Zhan, Sha Ou, Chao Zou, Min Zhao, and Chuan-De Wu*

Center for Chemistry of High-Performance and Novel Materials, Department of Chemistry, Zhejiang University, Hangzhou, 310027, P. R. China

Supporting Information

ABSTRACT: A flexible tripodal polyaromatic acid (4,4′,4″-(((2,4,6-trimethylbenzene-1,3,5-triyl)-tris(methylene))-tris-(oxy))tribenzoic acid, H_3TCM) was used to adapt the coordination sites of lanthanide ions for the construction of microporous lanthanide-organic frameworks (LOFs) $[LnTCM(H_2O)_2]\cdot 3DMF\cdot H_2O$ (Ln-TCM; Ln = La, Eu, and/or Tb). In these LOFs, the emission band of TCM matches well with the excitation energy of lanthanide ions (Eu^{3+} and Tb^{3+}) which results in high-efficient resonance energy transfer from TCM to lanthanide ions. Moreover, the mixed Eu_xTb_{1-x}–TCM has tunable pores to adapt different induced-fit-type host–guest interactions which can modulate both the energy transfer efficiency from TCM to Ln^{3+} ions and the energy allocation between Eu^{3+} and Tb^{3+} ions in the luminescence spectra. We demonstrate that the Eu_xTb_{1-x}–TCM sensor has the capability of decoding different volatile organic molecules (VOMs) with a clearly differentiable and unique emission intensity ratio of $^5D_0 \rightarrow {}^7F_2$ (Eu^{3+}, 614 nm) to $^5D_4 \rightarrow {}^7F_5$ (Tb^{3+}, 545 nm) transitions for every different VOM. Compared with the traditional absolute emission intensity method, such a self-referencing emission intensity strategy has generated self-calibrating, highly differentiable, and very stable luminescent signals for decoding different VOMs from the unique Eu_xTb_{1-x}–TCM platform, which has great potential for practical applications.

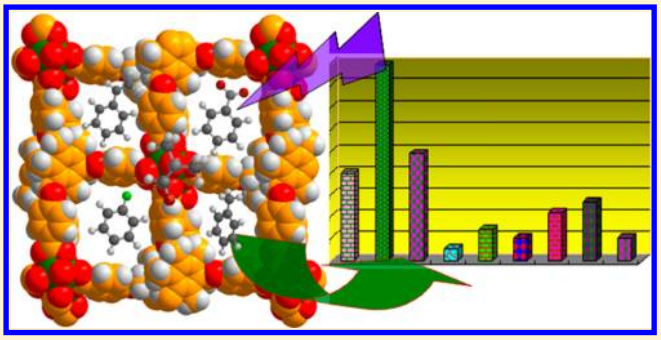

Probing small molecules is critical and challenging because it is significant and necessary in the fields of biotechnology, separation, and environmental monitoring.[1] However, given the fact that most of the volatile organic molecules (VOMs) have similar structural motifs and chemical and physical properties, probing small molecules with clearly differentiable and unique readouts remains a great challenge. Attracted by the unique electronic properties of lanthanide (Ln) ions originated from the 4f electrons, such as long luminescence lifetimes, sharp and stable emission bands, and large absorption and emission energy gaps, luminescent lanthanide complexes offer a great challenge and opportunity in terms of molecular sensing.[2] However, the Laporte-forbidden 4f–4f transition and the weak light absorption ability of lanthanide ions let lanthanide complexes suffer from low quantum yields, and therefore they do not have sufficient luminescent brightness for practical applications.[3,4]

As an emerging class of porous materials, the properties of metal–organic frameworks (MOFs) can be systematically designed and tuned by implanting different functional groups into the pore structures, and thus their applications in diverse fields can be realized.[5,6] Therefore, self-assembly of inorganic and organic luminescent moieties into porous MOFs has generated many unique luminescent materials.[7−13] Being an important class of MOF materials, lanthanide-organic frameworks (LOFs) have emerged with unique luminescent properties by synergizing the functionalities of MOFs and Ln ions.[11−13] Moreover, introduction of suitable organic chromophoric sensitizers into LOF materials will significantly enhance their light absorption ability to increase the luminescent brightness of Ln ions by "antennae effect."[4] Therefore, probing small molecules/ions can be realized by tuning the energy transfer efficiency from "antennae" to Ln ions through the host–guest interactions. Indeed, there have been a number of luminescent LOFs whose optical properties are highly responsive to the included guest molecules.[13] However, their luminescent signals are only prominent to specific molecules. The lack of the capability of differentiating multiple organic molecules should be ascribed to most of the luminescent LOF sensors explored until now that are only based on the emission intensities of single Ln^{3+} ions whose guest-responsive sensitivity is not acute enough.

Recent elaborations have proved that the soft MOFs, constructed from flexible organic ligands and/or containing at least two entanglement single nets, have interesting dynamic breathing properties.[14] Such porous materials have the induced-fit-type structural transformation property to entrap various guest molecules by tuning the pore sizes and shapes to adapt different host–guest interactions, while the guest-dependent

Received: April 14, 2014
Accepted: June 3, 2014
Published: June 3, 2014

   dx.doi.org/10.1021/ac5013442 | Anal. Chem. 2014, 86, 6648–6653

interactions can be further transduced into unique luminescent signals.[9] Moreover, the distinguishability of luminescent signals can be further improved by systematically modulating the ratios of lanthanide ions in mixed LOFs to realize their different luminescent light colors.[11] Herein, we report a series of microporous LOFs, $[LnTCM(H_2O)_2]\cdot 3DMF\cdot H_2O$ (Ln-TCM; Ln = La, Eu, and/or Tb), constructed from a flexible organic ligand, 4,4′,4″-(((2,4,6-trimethylbenzene-1,3,5-triyl)-tris-(methylene))-tris(oxy))tribenzoic acid (H_3TCM). It is remarkable that the host−guest interaction not only can tune the energy transfer efficiency from "antenna" organic species to Ln^{3+} ions but also is able to modulate the energy allocation between different Ln^{3+} ions in the luminescence spectra of mixed Ln-TCMs. The Eu^{3+} and Tb^{3+} codoped $Eu_{0.35}Tb_{0.65}$−TCM presents a remarkable property to confine different VOMs by undergoing induced-fit-type dynamic structural transformations and further emits unique and clearly differentiable photoluminescence for each and every VOM in the visible light region to simply realize decoding different VOMs.

RESULTS AND DISCUSSION

Colorless crystals of Ln-TCMs (Ln = La, Eu, and Tb) were synthesized by the reaction of H_3TCM and lanthanide nitrate in a mixed solvent of DMF and methanol heated at 50 °C for 2 days. The formulas of Ln-TCMs were established based on single crystal structures, elemental analyses, and thermogravimetric analyses (TGA). Single crystal X-ray diffraction analysis revealed that the three Ln-TCMs are isomorphous, which crystallize in the triclinic $P\bar{1}$ space group.[15] Herein, we only discuss the crystal structure of La-TCM in detail. There is one crystallographic La^{3+} ion, one TCM, and two water ligands in the asymmetric unit. As shown in Figure 1, two nine-coordinated La^{3+} ions are coupled in pairs by four TCM carboxylate groups to form a secondary building unit (SBU) $\{La_2(COO)_6(H_2O)_4\}$ ($\{La_2\}$), whereas TCM acts as a hexadentate ligand to coordinate with five La^{3+} ions. The further connection between $\{La_2\}$ SBUs and TCM ligands results in a double-layered coordination network. It is interesting that the neighboring gird layers are packed in an ···AA··· stacking fashion to generate a 3D supramolecular network, containing 1D opening channels with dimensions of about 12.3 × 12.5 $Å^2$ as viewed along the *a* axis. PLATON calculations indicate that Ln-TCMs consist of ∼40.3% void space to accommodate solvent molecules.[16]

As shown in the excitation and emission spectra of the powder samples of H_3TCM and La-TCM measured at room temperature (Figures S6 and S7), the free H_3TCM ligand displays an intense and broad band with a maximum at 360 nm in the emission spectrum under 300 nm UV light excitation, while the light emission peak of La-TCM shifts to 403 nm upon excitation at 305 nm. The red-shift of the emission of TCM in La-TCM should be attributed to the deprotonation and coordination of TCM with La^{3+} ions.[17] However, the light emission from TCM disappears in the luminescence spectra of Eu-TCM and Tb-TCM upon excitation at 285 nm (Figure 2). In contrast, Eu-TCM and Tb-TCM exhibit the characteristic strong and sharp lanthanide luminescence emission bands. Eu-TCM exhibits the characteristic emission bands of Eu^{3+} ions at 580, 592, 614, 653, and 701 nm in the luminescence spectrum, which are ascribed to the $^5D_0 \rightarrow {}^7F_0$, $^5D_0 \rightarrow {}^7F_1$, $^5D_0 \rightarrow {}^7F_2$, $^5D_0 \rightarrow {}^7F_3$, and $^5D_0 \rightarrow {}^7F_4$ transitions, respectively. Tb-TCM presents the characteristic transitions of Tb^{3+} ions in the luminescence spectrum, such as $^5D_4 \rightarrow {}^7F_6$ (490 nm), $^5D_4 \rightarrow {}^7F_5$ (545 nm), $^5D_4 \rightarrow {}^7F_4$ (584 nm), and $^5D_4 \rightarrow {}^7F_3$ (622 nm). It is interesting that the emission intensities of Eu-TCM and Tb-TCM are significantly enhanced compared with those excited at the characteristic wavelengths of 394 and 370 nm, respectively. These results suggest that the energy was very efficiently transferred from TCM to Eu^{3+} or Tb^{3+} ions by close matching of the emission energy of TCM and the excitation energy of Ln^{3+} ions via the "antenna effect." The quantum yields of 31.2 (Eu-TCM) and 73.6% (Tb-TCM) excited at 285 nm are significantly higher than that of 18.1% (Eu-TCM) excited at 394 nm and 5.1% (Tb-TCM) excited at 370 nm, respectively. These excellent values suggest that the light absorption, energy transfer, and emission rate are well balanced, which result in very intense luminescence from the efficient ligand-to-metal energy transfer and effective shielding of Ln^{3+} ions to prevent nonradiative decay.[18] The time-resolved emission profiles at 614 and 545 nm were also collected for Eu-TCM and Tb-TCM (λ_{ex} = 285 nm), respectively. The observed luminescent decay profiles correspond to the single exponential functions with the satisfactory agreement lifetime values of τ = 1.2 (Eu-TCM) and 0.79 (Tb-TCM) ms, thus implying the presence of only one emissive Ln^{3+} center in Ln-TCM.[10] Moreover, the emission intensity of Tb-TCM is systematically stronger than that of Eu-TCM excited at 285 nm, suggesting that the ligand-to-metal energy transfer from TCM to Tb^{3+} is more efficient than that from TCM to Eu^{3+}.[19]

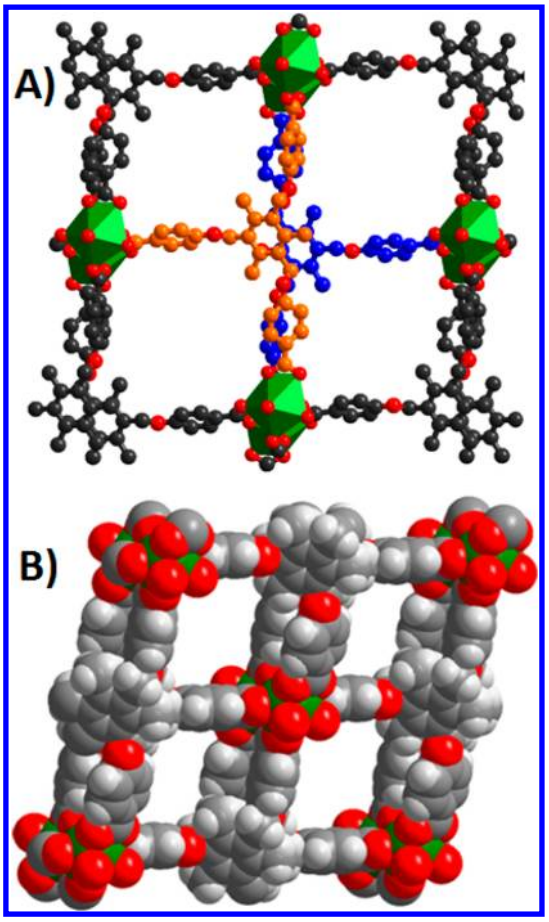

Figure 1. (a) A side view of the double-layered network of Ln-TCM. (b) Packing diagram of Ln-TCM as viewed along the *a* axis, showing the 1D opening channels (Color scheme: Ln, green; O, red; C, deep gray; H, light gray).

dx.doi.org/10.1021/ac5013442 | Anal. Chem. 2014, 86, 6648−6653

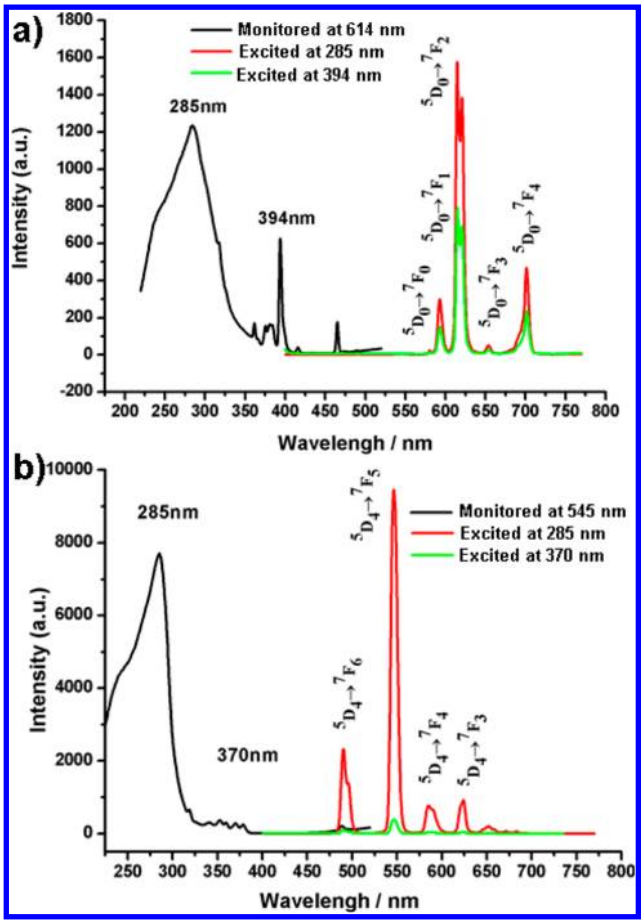

Figure 2. Excitation (black) and emission (green and red) spectra for Eu-TCM (a) and Tb-TCM (b).

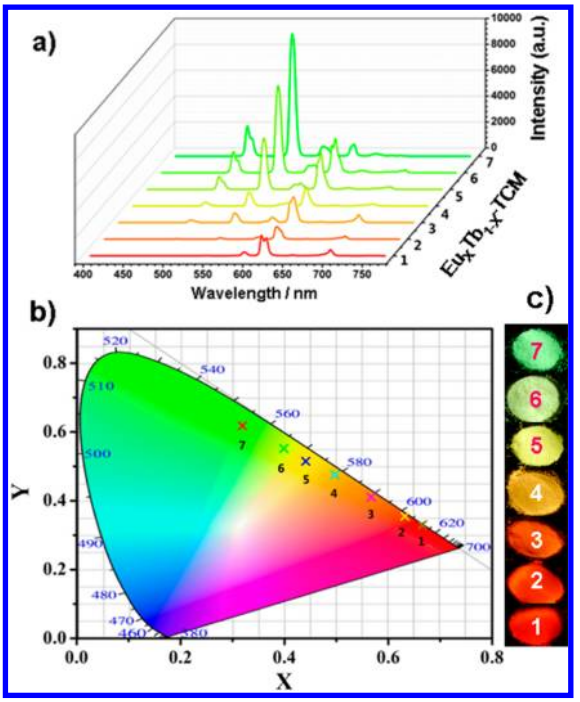

Figure 3. (a) Emission spectra of Eu_xTb_{1-x}-TCM (x = 1 (1); 0.65 (2); 0.4 (3); 0.35 (4); 0.25 (5); 0.1 (6); 0 (7)) in the solid-state at room temperature (λ_{ex} = 285 nm). (b) CIE chromaticity coordinates and (c) the corresponding optical photographs for Eu_xTb_{1-x}-TCM excited at 285 nm.

The luminescent colors of these isomorphous Ln-TCMs can be systematically tuned by modulating the ratios of Eu^{3+}/Tb^{3+} ions in the synthesis procedures. The structural identity of the codoped samples of Eu_xTb_{1-x}-TCM (x = 0.1, 0.25, 0.35, 0.4, 0.65) was confirmed by powder X-ray diffraction (PXRD) patterns, while the contents of Eu^{3+} and Tb^{3+} were determined by ICP-MS. As shown in Figure 3, the samples of Eu_xTb_{1-x}-TCM exhibit tunable light emission colors controlled by enhancing and weakening the corresponding emission intensities of Eu^{3+} and Tb^{3+} ions excited at 285 nm, respectively. The observed emission colors of Eu_xTb_{1-x}-TCM match well with the calculated chromaticity coordinates according to the 1931 Commission Internationale de L'Eclairage (CIE) chromaticity diagram.

Since the emission energy of Ln^{3+} ions in the luminescence spectra of Ln-TCMs is transferred from TCM by excitation, we expected that the transfer efficiency should be responsive to the included solvent molecules through host−guest interactions. Therefore, Ln-TCMs will exhibit guest-dependent luminescence and thus realize their application in decoding different VOMs. Considering that an ideal detector should have accessible pores by solvent molecules to facilitate solvent sensing, we have examined the porosity of La-TCM by CO_2 adsorption experiment. After a sample of La-TCM was activated by heating at 80 °C for 24 h, the activated La-TCM takes up 33 cm^3/g CO_2 at 0 °C, corresponding to the surface area of 250.6 m^2/g. PXRD peaks of the activated one are different from the freshly as-synthesized sample, indicating that some structural phase transformations might occur during the desolvation process because the ···AA··· stacked grid layers are loosely combined through weak supramolecular interactions. It is interesting that the PXRD pattern can be reversed to the original of La-TCM when a desolvated sample of La-TCM was exposed to the DMF vapor at 80 °C for 24 h. We further examined the access of different solvent molecules into the pores of the activated La-TCM by the sorption experiments. The activated samples of La-TCM were immersed in various different solvents for 12 h at room temperature to study the guest inclusion properties of La-TCM. UV−vis analysis indicates that the activated ones readily take up enough amounts of different solvent molecules such as benzene, styrene, chlorobenzene, nitrobenzene, benzyl alcohol, and aniline (Figure S14). PXRD peaks of these solvent included samples are slightly shifted depending on the included solvents. As shown in Table S3, the different unit cell parameters suggest that the positions and the pore structures based on the loosely combined grid layers can be tuned to adapt the supramolecular interactions between the LOF hosts and the included solvent guests by induced-fit-type interactions. When the solvent-included samples were exposed to the DMF vapor at 80 °C for 24 h, the sharp PXRD peaks of these samples are basically identical to that of the as-synthesized one which once again confirmed the flexible and reversible framework of Ln-TCM that is depending on the included solvent molecules (Figure S12). This type of guest-responsive structural transformations should play key roles in decoding different small organic molecules because the emission energy of Ln^{3+} ions in the luminescence spectra of Ln-TCMs is transferred from TCM by excitation at 285 nm.

Because the emission intensities of Eu^{3+} and Tb^{3+} ions in the luminescence spectrum of $Eu_{0.35}Tb_{0.65}$-TCM excited at 285 nm

dx.doi.org/10.1021/ac5013442 | Anal. Chem. 2014, 86, 6648−6653

are comparable, we have therefore studied the sensing property of $Eu_{0.35}Tb_{0.65}$-TCM for probing different VOMs. After the evacuated samples of $Eu_{0.35}Tb_{0.65}$-TCM were immersed in different solvents of benzene, styrene, benzyl alcohol, nitrobenzene, chlorobenzene, aniline, methanol, and DMF for 1 h, as shown in Figure 4, these solid samples exhibit solvent-dependent fluorescences. For example, nitrobenzene exhibits a significant quenching effect for the emissions of both Eu^{3+} and Tb^{3+} ions, while styrene and benzyl alcohol mainly quench the emission of Tb^{3+} ions. Chlorobenzene exhibits an enhancing effect for the emission of Eu^{3+} ions, while DMF presents an enhancing effect for both emissions of Eu^{3+} and Tb^{3+} ions. Such enhancing and quenching effects make $Eu_{0.35}Tb_{0.65}$-TCM emit solvent-dependent light colors, even clearly distinguishable by the naked eye.

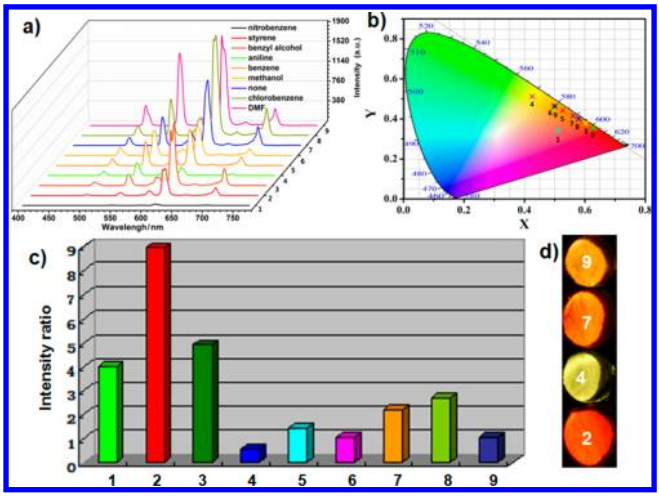

Figure 4. (a) Emission spectra, (b) CIE chromaticity coordinates, (c) the integrated emission intensity ratios of $^5D_0 \rightarrow {}^7F_2$ (Eu^{3+}, 614 nm) to $^5D_4 \rightarrow {}^7F_5$ (Tb^{3+}, 545 nm) transitions and (d) the selected optical photographs for $Eu_{0.35}Tb_{0.65}$-TCM after adsorption of nitrobenzene (1), styrene (2), benzyl alcohol (3), aniline (4), benzene (5), methanol (6), none (7), chlorobenzene (8), and DMF (9) molecules excited at 285 nm.

The above results clearly demonstrate that the luminescent colors and the absolute emission intensities of $Eu_{0.35}Tb_{0.65}$-TCM are responsive to the included VOMs by tuning the energy transfer efficiency from TCM to Eu^{3+} and/or Tb^{3+} ions. However, the enhancing or quenching effect for the absolute emission intensity of a single Ln^{3+} ion transition, such as Eu^{3+}, is inconspicuous for differentiating some VOMs, such as benzyl alcohol and benzene, chlorobenzene, and DMF, which is often observed in the luminescence spectra of MOF sensors.[8] It is remarkable that these solvent molecules can be easily differentiated by monitoring the emission intensity ratios of $^5D_0 \rightarrow {}^7F_2$ (Eu^{3+}, 614 nm) to $^5D_4 \rightarrow {}^7F_5$ (Tb^{3+}, 545 nm) transitions in the luminescence spectra of $Eu_{0.35}Tb_{0.65}$-TCM (Figure 4c). These results indicate that the included small organic molecules not only can tune the energy transfer efficiency from "antenna" organic species to Eu^{3+}/Tb^{3+} ions but also are able to modulate the energy allocation between Eu^{3+} and Tb^{3+} ions in the luminescence spectra of mixed LOFs by the induced-fit-type host−guest interactions. Therefore, the tunable energy allocation between Eu^{3+} and Tb^{3+} ions in the luminescence spectra of mixed LOFs will enhance the emission of one Ln^{3+} ion and weaken the emission of another Ln^{3+} ion. Compared with a LOF sensor containing only one kind of Ln^{3+} ions, such a self-referring strategy can enlarge the relative emission ratio, which will amplify the luminescent signals in probing different VOMs and let probing different VOMs be easily realized. Such a self-referring strategy is more reliable than the absolute emission intensity method in probing different VOMs because the solid-state emission intensities have many uncontrollable errors. The superiority is very conspicuous in the recycle probing of aniline molecules by the solid sample of $Eu_{0.35}Tb_{0.65}$-TCM (Figure S23). The absolute emission intensity of the characteristic transition of $^5D_0 \rightarrow {}^7F_2$ (614 nm) for Eu^{3+} ions is variable in nine cycles, even though its structure is basically intact as confirmed by PXRD patterns. It is remarkable that the relative emission intensity of $^5D_0 \rightarrow {}^7F_2$ (Eu^{3+}, 614 nm) to $^5D_4 \rightarrow {}^7F_5$ (Tb^{3+}, 545 nm) transitions is almost invariant for nine cycles. The above results clearly demonstrate that $Eu_{0.35}Tb_{0.65}$-TCM has a self-calibrating property in sensing VOMs, which is amenable to overcoming the unstable and insensitive drawbacks of the method based on the absolute solid-state emission intensities of single Ln^{3+} ions.

It is very important that the characteristic emission intensity ratio of $^5D_0 \rightarrow {}^7F_2$ (Eu^{3+}, 614 nm) to $^5D_4 \rightarrow {}^7F_5$ (Tb^{3+}, 545 nm) transitions is invariant to the same guest and variable to different solvent molecules. The different solvent-dependent emission ratios in the luminescence spectra of the same mixed LOFs have enabled them to be excellent candidates as the self-calibrating luminescent sensors by fingerprint correlation between the relative emission intensity and each and every different solvent molecule. As shown in Figure 4c, each guest molecule has a unique emission intensity ratio of $^5D_0 \rightarrow {}^7F_2$ (614 nm) to $^5D_4 \rightarrow {}^7F_5$ (545 nm) transitions in the luminescence spectra of $Eu_{0.35}Tb_{0.65}$-TCM. Remarkably, as shown in Figure 5, the small molecules, having very similar structural motifs, are unambiguously decoded by the self-referring strategy, such as isomerides of *o*-, *m*-, and *p*-xylene; homologens of benzene, toluene, and ethylbenzene; and halogeno-benzenes of fluoro-, chloro-, bromo-, and iodo-benzene.

CONCLUSIONS

In summary, we demonstrate that the Ln-TCM can tune the pore structures to adapt the induced-fit-type interactions between the included guest molecules and host LOF matrices. Moreover, the emission band of TCM matches well with the excitation bands of Eu^{3+} and Tb^{3+} ions, which achieves highly efficient resonance energy transfer from ligands to lanthanide ions in the luminescence spectra of Ln-TCM (Ln = Eu^{3+} and/or Tb^{3+}). The energy transfer efficiency from TCM to Ln^{3+} ions and the energy allocation around different Ln^{3+} ions are highly responsive to the induced-fit-type host−guest interactions. Therefore, probing different VOMs is simply realized by transducing the unique host−guest interactions into characteristic luminescent readouts of the emission ratios between Eu^{3+} and Tb^{3+} ions. The codoped Eu_xTb_{1-x}-TCM can even distinguish structurally similar molecules, such as isomerides of *o*-, *m*-, and *p*-xylene; homologens of benzene, toluene, and ethylbenzene; and halogeno-benzenes of fluoro-, chloro-, bromo-, and iodo-benzene. Such an internal label strategy is not only amenable to overcoming the random errors of the solid-state fluorescence but also able to amplify the luminescent signals by introducing the self-calibrating luminescent centers. These results represent the first example of LOF materials that can clearly decode different VOMs from one another. We

dx.doi.org/10.1021/ac5013442 | Anal. Chem. 2014, 86, 6648−6653

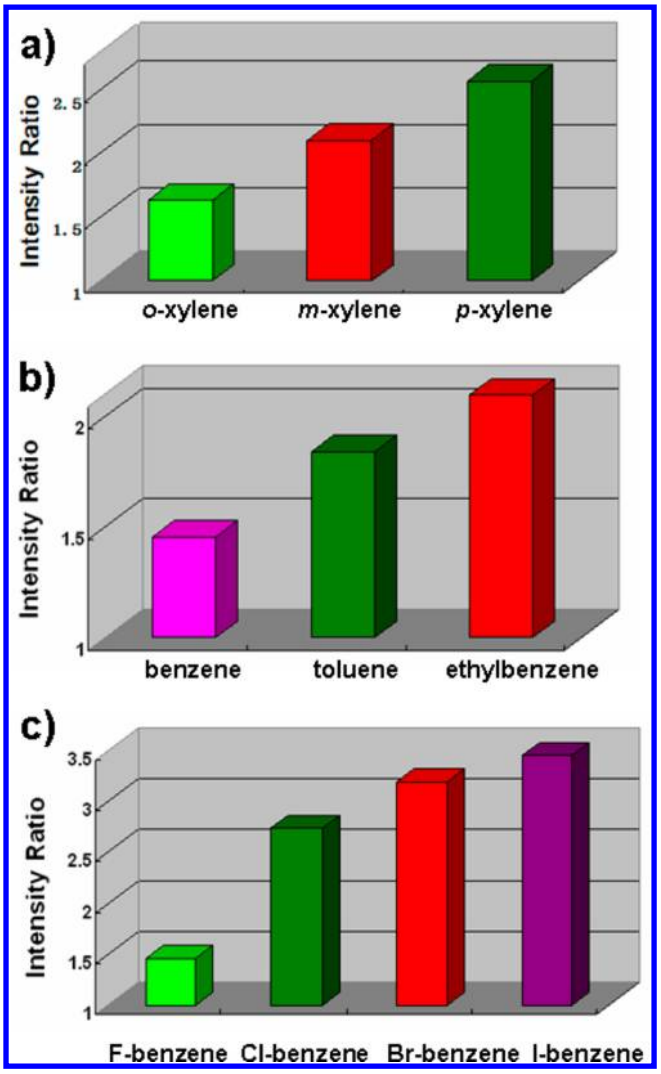

Figure 5. Emission intensity ratios of $^5D_0 \rightarrow {}^7F_2$ to $^5D_4 \rightarrow {}^7F_5$ transitions in the luminescence spectra of $Eu_{0.35}Tb_{0.65}$-TCM excited at 285 nm after adsorption of (a) isomerides of *o*-, *m*-, and *p*-xylene; (b) homologens of benzene, toluene, and ethylbenzene; and (c) halogenobenzenes of fluoro-, chloro-, bromo-, and iodo-benzene.

expect that our findings on the fingerprint luminescence responses of the mixed LOFs toward different analytes will prompt the development of versatile luminescent materials for practical applications in the near future.

EXPERIMENTAL SECTION

Materials and Methods. All reagents and solvents were obtained from commercial sources and used as supplied without further purification, except H_3TCM was synthesized according to the literature.[20] FT-IR spectra were recorded from KBr pellets on an FTS-40 spectrophotometer. PXRD were recorded on a RIGAKU D/MAX 2550/PC for Cu Kα radiation (λ = 1.5406 Å). TGA were carried out under a N_2 atmosphere on a NETZSCH STA 409 PC/PG instrument at a heating rate of 10 °C min^{-1}. Elemental analyses were performed on a ThermoFinnigan Flash EA 1112 elementary analyzer. Inductively coupled plasma mass spectrometry (ICP-MS) was performed on an XSeries II instrument. A Micromeritics ASAP 2020 surface area analyzer was used to measure CO_2 gas adsorption isotherms. Luminescence spectra of the solid samples were recorded on a Hitachi F4600 fluorescence spectrometer at room temperature. The ground crystalline solid samples (3 mg) were sealed in a 2 × 10 mm^2 flat quartz cylinder cell. The photomultiplier tube voltage is 500 V, and the scan speed is 1200 nm min^{-1}, while the slit widths of excitation and emission spectra are both 2.5 nm. The luminescence decay curves were measured with an Edinburgh Instrument F900, and both the excitation and emission slits are 2.0 nm.

Synthesis of $[LaTCM(H_2O)_2]\cdot 3DMF\cdot H_2O$ (La-TCM). La$(NO_3)_3\cdot 6H_2O$ (3 mg, 0.007 mmol) and H_3TCM (3 mg, 0.0053 mmol) were dissolved in DMF (2 mL) and methanol (3 mL). The mixture was sealed in a screw cap vial and heated at 50 °C for 2 days. Colorless crystals of La-TCM were collected by filtration, washed with DMF and methanol, and dried at room temperature. Yield: 3.5 mg (67% based on H_3TCM). Anal. Calcd for $C_{42}H_{54}N_3LaO_{15}$ (%): C, 51.49; H, 5.56; N, 4.29. Found (%): C, 51.05; H, 5.68; N, 4.21. FTIR (KBr pellet): ν/cm^{-1} 1655(s), 1604(s), 1537(s), 1510(m), 1416(s), 1302(m), 1240(s), 1173(s), 1142(w), 1104(m), 1027(w), 991(s), 861(m), 787(m), 701(w), 674(w), 648(w), 635(w), 619(w), 605(w), 556(w), 409(m).

Synthesis of $[Eu_xTb_{1-x}TCM(H_2O)_2]\cdot 3DMF\cdot H_2O$ (x = 0, 0.1, 0.25, 0.35, 0.4, 0.65, 1). Similar processes were employed by adding certain amounts of corresponding lanthanide salts of $Eu(NO_3)_3\cdot 6H_2O$ and/or $Tb(NO_3)_3\cdot 6H_2O$. Anal. Calcd for $C_{42}H_{54}N_3EuO_{15}$ (Eu-TCM) (%): C, 50.81; H, 5.48; N, 4.23. Found (%): C, 49.95; H, 5.69; N, 4.13. FTIR (KBr pellet): ν/cm^{-1} 1654(s), 1604(s), 1534(m), 1511(w), 1420(s), 1301(m), 1240(s), 1172(s), 1144(w), 1105(m), 1026(w), 989(s), 867(m), 786(m), 701(w), 680(w), 650(w), 634(w), 605(w), 551(w), 410(w). Anal. Calcd for $C_{42}H_{54}N_3TbO_{15}$ (Tb-TCM) (%): C, 50.45; H, 5.44; N, 4.20. Found (%): C, 50.03; H, 5.48; N, 4.05. FTIR (KBr pellet): ν/cm^{-1} 1654(s), 1604(s), 1534(m), 1511(w), 1420(s), 1300(m), 1239(s), 1172(s), 1147(w), 1104(m), 1026(w), 989(s), 867(m), 785(m), 701(w), 680(w), 650(w), 634(w), 606(w), 553(w), 414(w).

A Typical Procedure for the Adsorption of Solvent Molecules. An activated sample of La-TCM (5 mg) was added to 0.3 mL of benzene at room temperature. After 12 h, the mixture was centrifugated, and the solid sample was washed with ethyl ether several times to remove the surface adsorbed solvent molecules. The solid sample was subsequently immersed in 5 mL of methanol for 1 h to exchange the included solvent molecules in the pores. The plasma was diluted into an appropriate concentration and analyzed with UV−vis absorption spectroscopy.

ASSOCIATED CONTENT

Supporting Information

Additional experimental procedures, additional figures, crystal data, scheme, tables, and CIF files. This material is available free of charge via the Internet at http://pubs.acs.org.

AUTHOR INFORMATION

Corresponding Author

*E-mail: cdwu@zju.edu.cn.

Notes

The authors declare no competing financial interest.

dx.doi.org/10.1021/ac5013442 | *Anal. Chem.* 2014, 86, 6648−6653

■ ACKNOWLEDGMENTS

We are grateful for the financial support of the National NSF of China (Grant Nos. 21373180 and J1210042) and Zhejiang Provincial Natural Science Foundation of China (Grant No. Z4100038).

■ REFERENCES

(1) (a) Haupt, K.; Mosbach, K. *Chem. Rev.* **2000**, *100*, 2495−2504. (b) McQuade, D. T.; Pullen, A. E.; Swager, T. M. *Chem. Rev.* **2000**, *100*, 2537−2574. (c) Beer, P. D.; Gale, P. A. *Angew. Chem., Int. Ed.* **2001**, *40*, 486−516.

(2) (a) Eliseeva, S. V.; Bünzli, J-C. G. *Chem. Soc. Rev.* **2010**, *39*, 189−227. (b) Montgomery, C. P.; Murray, B. S.; New, E. J.; Pal, R.; Parker, D. *Acc. Chem. Res.* **2009**, *42*, 925−937.

(3) (a) Bünzli, J.-C. G.; Piguet, C. *Chem. Soc. Rev.* **2005**, *34*, 1048−1077. (b) Binnemans, K. *Chem. Rev.* **2009**, *109*, 4283−4374.

(4) Moore, E. G.; Samuel, A. P. S.; Raymond, K. N. *Acc. Chem. Res.* **2009**, *42*, 542−552.

(5) Themed issues on metal-organic frameworks: Long, J. R.; Yaghi, O. M. *Chem. Soc. Rev.* **2009**, *38*, 1213−1504.

(6) Metal-Organic Frameworks special issue: Zhou, H.-C.; Long, J. R.; Yaghi, O. M. *Chem. Rev.* **2012**, *112*, 673−1268.

(7) (a) Allendorf, M. D.; Bauer, C. A.; Bhakta, R. K.; Houk, R. J. T. *Chem. Soc. Rev.* **2009**, *38*, 1330−1352. (b) Chen, B.; Xiang, S.; Qian, G. *Acc. Chem. Res.* **2010**, *43*, 1115−1124. (c) Lan, A.; Li, K.; Wu, H.; Olson, D. H.; Emge, T. J.; Ki, W.; Hong, M.; Li, J. *Angew. Chem., Int. Ed.* **2009**, *48*, 2334−2338. (d) Jiang, H.-L.; Tatsu, Y.; Lu, Z.-H.; Xu, Q. *J. Am. Chem. Soc.* **2010**, *132*, 5586−5587. (e) Lee, E. Y.; Jang, S. Y.; Suh, M. P. *J. Am. Chem. Soc.* **2005**, *127*, 6374−6381. (f) Fang, Q.-R.; Zhu, G.-S.; Jin, Z.; Ji, Y.-Y.; Ye, J.-W.; Xue, M.; Yang, H.; Wang, Y.; Qiu, S.-L. *Angew. Chem., Int. Ed.* **2007**, *46*, 6638−6642. (g) Li, Y.; Zhang, S.; Song, D. *Angew. Chem., Int. Ed.* **2013**, *52*, 710−713. (h) Xie, Z.; Ma, L.; deKrafft, K. E.; Jin, A.; Lin, W. *J. Am. Chem. Soc.* **2010**, *132*, 922−923. (i) An, J.; Shade, C. M.; Chengelis-Czegan, D. A.; Petoud, S. p.; Rosi, N. L. *J. Am. Chem. Soc.* **2011**, *133*, 1220−1223. (j) Stylianou, K. C.; Heck, R.; Chong, S. Y.; Bacsa, J.; Jones, J. T. A.; Khimyak, Y. Z.; Bradshaw, D.; Rosseinsky, M. J. *J. Am. Chem. Soc.* **2010**, *132*, 4119−4130. (k) McManus, G. J.; Perry, J. J., IV; Perry, M.; Wagner, B. D.; Zaworotko, M. J. *J. Am. Chem. Soc.* **2007**, *129*, 9094−9101. (l) Wang, M.-S.; Guo, S.-P.; Li, Y.; Cai, L.-Z.; Zou, J.-P.; Xu, G.; Zhou, W.-W.; Zheng, F.-K.; Guo, G.-C. *J. Am. Chem. Soc.* **2009**, *131*, 13572−13573.

(8) Cui, Y.; Yue, Y.; Qian, G.; Chen, B. *Chem. Rev.* **2012**, *112*, 1126−1162.

(9) (a) Takashima, Y.; Martínez, V. M.; Furukawa, S.; Kondo, M.; Shimomura, S.; Uehara, H.; Nakahama, M.; Sugimoto, K.; Kitagawa, S. *Nat. Commun.* **2011**, *2*, 168−175. (b) Dong, M.-J.; Zhao, M.; Ou, S.; Zou, C.; Wu, C.-D. *Angew. Chem., Int. Ed.* **2014**, *53*, 1575−1579.

(10) Harbuzaru, B. V.; Corma, A.; Rey, F.; Atienzar, P.; Jordá, J. L.; García, H.; Ananias, D.; Carlos, L. D.; Rocha, J. *Angew. Chem., Int. Ed.* **2008**, *47*, 1080−1083.

(11) (a) Cui, Y.; Xu, H.; Yue, Y.; Guo, Z.; Yu, J.; Chen, Z.; Gao, J.; Yang, Y.; Qian, G.; Chen, B. *J. Am. Chem. Soc.* **2012**, *134*, 3979−3982. (b) Guo, H.; Zhu, Y.; Qiu, S.; Lercher, J. A.; Zhang, H. *Adv. Mater.* **2010**, *22*, 4190−4192.

(12) (a) Chen, B.; Wang, L.; Xiao, Y.; Fronczek, F. R.; Xue, M.; Cui, Y.; Qian, G. *Angew. Chem., Int. Ed.* **2009**, *48*, 500−503. (b) Wang, P.; Ma, J.-P.; Dong, Y.-B.; Huang, R.-Q. *J. Am. Chem. Soc.* **2007**, *129*, 10620−10621. (c) White, K. A.; Chengelis, D. A.; Gogick, K. A.; Stehman, J.; Rosi, N. L.; Petoud, S. *J. Am. Chem. Soc.* **2009**, *131*, 18069−18071.

(13) (a) Chen, B.; Wang, L.; Zapata, F.; Qian, G.; Lobkovsky, E. B. *J. Am. Chem. Soc.* **2008**, *130*, 6718−6719. (b) Harbuzaru, B. V.; Corma, A.; Rey, F.; Jordá, J. L.; Ananias, D.; Carlos, L. D.; Rocha, J. *Angew. Chem., Int. Ed.* **2009**, *48*, 6476−6479. (c) Park, Y. K.; Choi, S. B.; Kim, H.; Kim, K.; Won, B.-H.; Choi, K.; Choi, J.-S.; Ahn, W.-S.; Won, N.; Kim, S.; Jung, D. H.; Choi, S.-H.; Kim, G.-H.; Cha, S.-S.; Jhon, Y. H.; Yang, J. K.; Kim, J. *Angew. Chem., Int. Ed.* **2007**, *46*, 8230−8233. (d) Wong, K. L.; Law, G. L.; Yang, Y. Y.; Wong, W. T. *Adv. Mater.* **2006**, *18*, 1051−1054. (e) Chen, B.; Yang, Y.; Zapata, F.; Lin, G.; Qian, G.; Lobkovsky, E. B. *Adv. Mater.* **2007**, *19*, 1693−1696.

(14) (a) Férey, G.; Serre, C. *Chem. Soc. Rev.* **2009**, *38*, 1380−1399. (b) Horike, S.; Shimomura, S.; Kitagawa, S. *Nat. Chem.* **2009**, *1*, 695−704.

(15) Crystal data for La-TCM: $C_{33}H_{31}LaO_{11}$, M = 742.49, triclinic, space group $P\bar{1}$, a = 9.168(2) Å, b = 13.570(2) Å, c = 17.837(4) Å, α = 86.18(1)°, β = 87.02(2)°, γ = 84.41(1)°, V = 2201.5(7) Å^3, Z = 2, μ = 1.014 mm^{-1}, R_1 = 0.0609, wR_2 = 0.1412, S = 1.022. For Eu-TCM: $C_{33}H_{31}EuO_{11}$, M = 755.54, triclinic, space group $P\bar{1}$, a = 9.1035(6) Å, b = 13.6438(9) Å, c = 17.732(1) Å, α = 87.620(5)°, β = 85.388(5)°, γ = 86.422(5)°, V = 2189.5(2) Å^3, Z = 2, μ = 10.626 mm^{-1}, R_1 = 0.0756, wR_2 = 0.1619, S = 1.034. For Tb-TCM: $C_{33}H_{31}TbO_{11}$, M = 762.50, triclinic, space group $P\bar{1}$, a = 9.1308(3) Å, b = 13.6503(4) Å, c = 17.7229(5) Å, α = 87.558(2)°, β = 85.382(3)°, γ = 86.398(3)°, V = 2195.9(1) Å^3, Z = 2, μ = 8.291 mm^{-1}, R_1 = 0.0382, wR_2 = 0.0985, S = 1.022.

(16) Spek, A. L. *PLATON, a multipurpose crystallographic tool*; Utrecht University: Utrecht, The Netherlands, 2008.

(17) Lakowicz, J. R. *Principles of Fluorescence Spectroscopy*, 3rd ed.; Springer: Berlin, 2006.

(18) Chatterton, N.; Bretonnière, Y.; Pécaut, J.; Mazzanti, M. *Angew. Chem., Int. Ed.* **2005**, *44*, 7595−7598.

(19) Brites, C. D. S.; Lima, P. P.; Silva, N. J. O.; Millán, A.; Amaral, V. S.; Palacio, F.; Carlos, L. D. *Adv. Mater.* **2010**, *22*, 4499−4504.

(20) Zhan, C.; Zou, C.; Kong, G.-Q.; Wu, C.-D. *Cryst. Growth Des.* **2013**, *13*, 1429−1437.